Enhanced charge efficiency and reduced energy use
in capacitive deionization by increasing the discharge voltage

T. Kim,[1,2] J.E. Dykstra,[1,3] S. Porada,[1] A. van der Wal,[3] J. Yoon,[2] P.M. Biesheuvel[1,4]

[1]*Wetsus, centre of excellence for sustainable water technology, Oostergoweg 7, 8911 MA Leeuwarden, The Netherlands*. [2]*School of Chemical and Biological Engineering, Institute of Chemical Processes, Seoul National University, Daehak-dong, Gwanak-gu, Seoul 151-742, Republic of Korea*. [3]*Department of Environmental Technology, Wageningen University, Bornse Weilanden 9, 6708 WG Wageningen, The Netherlands*. [4]*Laboratory of Physical Chemistry and Colloid Science, Wageningen University, Dreijenplein 6, 6703 HB Wageningen, The Netherlands.*

Abstract

Capacitive deionization (CDI) is an electrochemical method for water desalination using porous carbon electrodes. A key parameter in CDI is the charge efficiency, Λ, which is the ratio of salt adsorption over charge in a CDI-cycle. Values for Λ in CDI are typically around 0.5-0.8, significantly less than the theoretical maximum of unity, due to the fact that not only counterions are adsorbed into the pores of the carbon electrodes, but at the same time coions are released. To enhance Λ, ion-exchange membranes (IEMs) can be implemented. With membranes, Λ can be close to unity because the membranes only allow passage for the counterions. Enhancing the value of Λ is advantageous as this implies a lower electrical current and (at a fixed charging voltage) a reduced energy use. We demonstrate how, without the need to include IEMs, the charge efficiency can be increased to values close to the theoretical maximum of unity, by increasing the cell voltage during discharge, with only a small loss of salt adsorption capacity per cycle. In separate constant-current CDI experiments, where after some time the effluent salt concentration reaches a stable value, this value is reached earlier with increased discharge voltage. We compare the experimental results with predictions of porous electrode theory which includes an equilibrium Donnan electrical double layer model for salt adsorption in carbon micropores. Our results highlight the potential of modified operational schemes in CDI to increase charge efficiency and reduce energy use of water desalination.

Introduction

Capacitive deionization is an electrochemical method for water desalination based on applying a voltage difference (called the cell voltage, V_{cell}, or charging voltage, V_{ch}) between two porous carbon electrode films in contact with aqueous electrolyte [1,2,3,4,5,6,7,8,9]. In this process, ions migrate to the electrode of opposite charge (cations to the cathode, anions to the anode) following charge transfer through the external circuit that connects the two electrodes. Within the electrode, ions are stored in the electrical double layers (EDL) which form in the micropores inside the porous carbon particles that compose the electrode [10]. As a consequence, the water flowing through the cell becomes partially desalinated. Generally, the two electrode films are placed parallel to the direction of water flow which runs in between the electrodes through a spacer layer, see Fig. 1a. Alternative designs use carbon electrode wires [11], flowable electrode slurries [12,13,14,15,16] or flow-through

electrodes [17]. In addition, electrodes can be chemically modified [18,19], nanoparticles can be incorporated [20,21,22], ion-selective coatings can be applied [23,24], or ion-exchange membranes can be placed in front of the electrodes in a modification called Membrane Capacitive Deionization, or MCDI [25,26,27,28,29,30,31,32].

In most of these designs, CDI comprises a repeated cycle of charging (salt adsorption) and discharging (salt release), where salt ions are adsorbed upon applying a cell voltage during charging. After subsequent discharge of the cell, generally done by short-circuiting the two electrodes (i.e., a discharge voltage of V_{disch}=0 V is applied), ions are released from the electrodes and a concentrated saline stream is temporarily produced. These two steps of salt adsorption (charging) and desorption (discharge) constitute one full CDI cycle. The charge efficiency Λ describes the ratio of salt adsorption (desorption) over the charge transfer [5,8,22,33,34,35]. The charge efficiency Λ differs between materials and depends on the applied cell voltage and salt concentration [36]. For a typical cell voltage of V_{cell}=1.2 V and for salt concentrations in the range 5-50 mM, values for Λ ranging from 0.5 to 0.8 have been experimentally found. Charge efficiency Λ increased with cell voltage, and decreased with salt concentration [36]. Values for Λ close to, or beyond, unity have never been reported for CDI. Indeed, a value of Λ of unity is considered the theoretical maximum, and would be achieved when one full NaCl salt molecule is removed for an equivalent electron transfer between the electrodes. The lower values of Λ obtained in practice, are disadvantageous as it implies more charge transfer and electrical energy input than is necessary for a given objective of salt removal. However, such sub-optimal values of Λ clearly below unity seem to be inherently connected to CDI as a consequence of the structure of the electrical double layer (EDL) in microporous carbons, where the electrical charge is partially compensated by counterion adsorption, and partially by coion repulsion (ejection of coions from the EDL) [36]. The repulsion of the coions results in sub-optimal values of the charge efficiency, i.e. a charge efficiency below unity. For salt concentrations below 30 mM, implementation of ion-exchange membranes increases the charge efficiency Λ (see Fig. 5d in ref. 25) to values close to one, because coions are blocked from leaving the electrode region, and only counterions are transported from spacer to electrode to compensate the electronic charge. The disadvantage of membrane-CDI is the more expensive cell design. Though not well supported by experimental data, theoretical calculations suggest that another route to reach a higher charge efficiency, is to increase the charging voltage to values beyond 1.2 V [36]. However, because of water splitting, voltages beyond 1.23 V lead to an increase in leakage currents, that is, a current which results in electrochemical reactions, which is not used to charge the porous carbon electrodes. Therefore, cell voltages beyond 1.23 V may result in a higher energy consumption. Also the use of (chemically modified) asymmetric electrodes, and reference electrodes, has been suggested as methods to increase Λ [18].

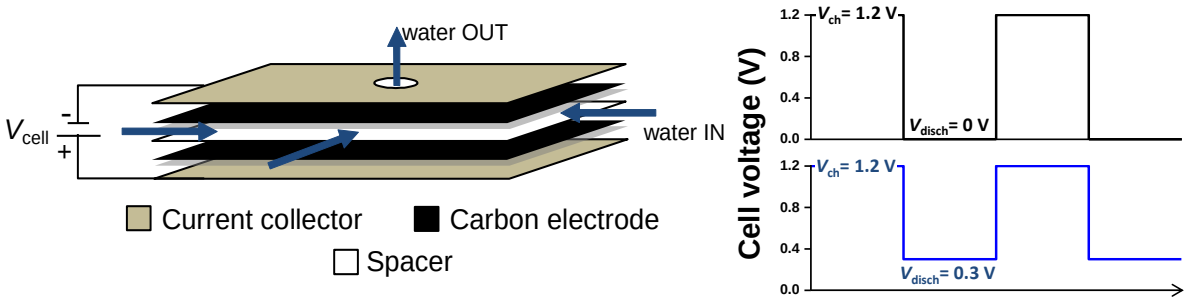

Fig. 1. (a) Schematic diagram of a CDI cell as used in this study. (b) Operational cycles where discharge voltage is varied (V_{disch} = 0 V and 0.3 V) as a function of time.

To increase charge efficiency, another route is the use of an increased discharge voltage and, as a consequence, a smaller voltage window for CDI as has been suggested and tested before [37]. This is the route we will reanalyze and extend in the present work by using a fixed value of the cell voltage during charging, V_{ch}=1.2 V, just below the water-splitting voltage, and increase the discharge voltage, V_{disch}, to values above zero, see Fig. 1b. As we will demonstrate, both experimentally and theoretically, increasing V_{disch} only moderately, to around V_{disch}=0.3 V, leads to increased values of Λ, while at the same time the salt adsorption capacity and salt adsorption rate are not affected much (order of 5%). Because of the reduced voltage window used in our study, the total charge transfer in one cycle decreases significantly, and thus the overall energy consumption is lower. For instance, in our setup, and for c_{salt}=20 mM and V_{ch}=1.2 V, the energy requirement per ion removed reduces from ~30 kT per ion when V_{disch}=0 V, to ~26 kT per ion when V_{disch}=0.3 V. The results presented in this work go beyond the pioneering work reported in ref. [37] where the charging voltage was V_{ch}=0.6 V and therefore charge efficiency Λ still stayed far below unity, increasing from Λ=0.4 to Λ=0.7 upon increasing the discharge voltage from V_{disch}=0 V to 0.4 V. Another difference is that in refs. [37,38] it was argued that increasing V_{disch} is disadvantageous because of a significant decrease in salt removal per cycle. However, as we will show, when V_{ch} is the value that we use, V_{ch}=1.2 V, then in the relevant range of values of V_{disch} (up to 0.3 V), this decrease is minor.

In addition, we demonstrate that theoretical equilibrium calculations using a recently proposed “improved modified” Donnan (i-mD) model [36] closely fit the data for charge transfer and salt adsorption, across a range of values of cell voltage and salt concentration, while a porous electrode transport theory for CDI well illustrates dynamic data, i.e., ion transport rates in CDI. We also present experimental and theoretical results for constant-current charging in CDI [39], demonstrating that with an increased discharge voltage the transition period required to reach a stable effluent salinity can be drastically reduced. In summary, our results demonstrate the possibility to increase the charge efficiency in a CDI cycle to values close to unity, leading to a lowered energy consumption, and unchanged salt adsorption, by raising the discharge voltage in CDI to values higher than zero.

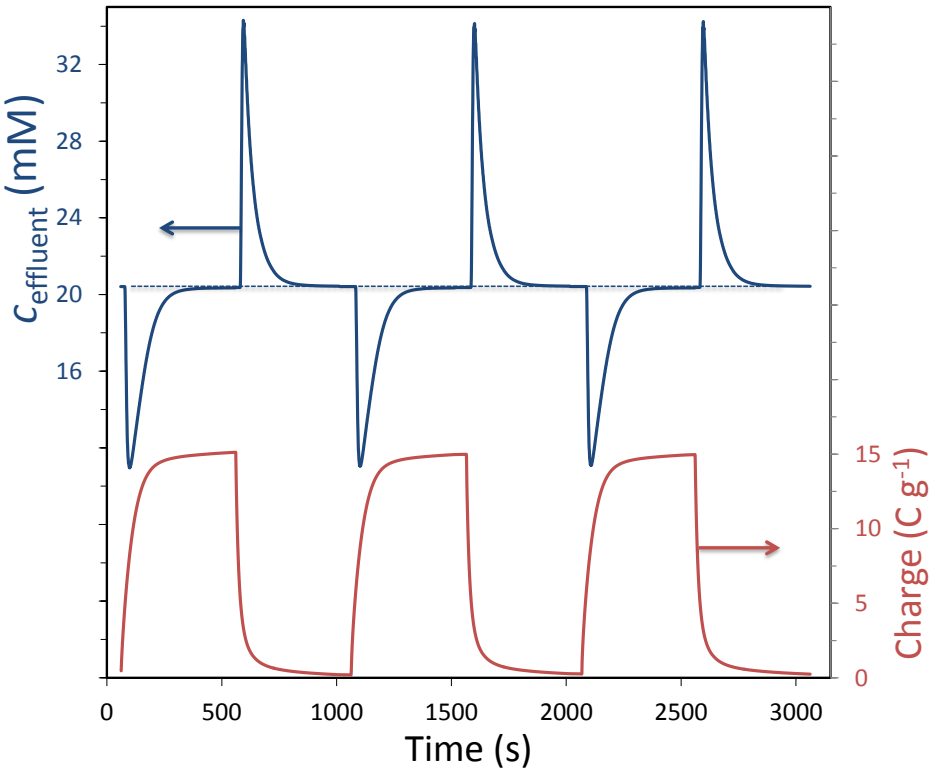

Fig 2. Experimental data of CDI cycles for effluent salt concentration and accumulated charge, versus time (V_{ch}=1.2 V, V_{disch}=0.3 V, c_{∞}=20 mM, half-cycle time 1200 s, only first 500 s shown).

Theory

Equilibrium EDL model. To rationalize the origin of improved charge efficiency in a CDI cycle, we make use of an electrical double layer (EDL) model for ion adsorption in microporous carbons [35]. Here we will use the improved modified Donnan (i-mD) model [36] which is an EDL-model that assumes full overlap of the diffuse layers in the small micropores [1,36]. The i-mD model does not consider ion size effects, but does include a Stern layer capacity and a non-classical "μ_{att}"-term that describes how uncharged carbon micropores also adsorb salt. The EDL model describes the ion concentrations inside the intraparticle pore space, or micropores, ("mi"), where we model the formation of the EDL and the adsorption of salt, as function of the concentration outside the carbon particles (interparticle pore space, or macropores, "mA") [40], which we model as transport pathways for ions to move from the external solution outside the electrode to the micropores. Note that in this work, the terminology micro-, meso- and macropores, is based on their use in porous electrode transport theory [1,41] which is a nomenclature different from the strict distinction in size classes as in the IUPAC-definition. At equilibrium, there is no transport across the electrode, and this macropore concentration is equal to that of the external solution outside the electrode, which we will describe using the subscript "∞".

For a 1:1 salt such as NaCl, in the i-mD model the micropore ion concentration relates to that outside the pores according to a modified Boltzmann equilibrium,

$$c_{mi,i} = c_{\infty} \cdot \exp\left(-z_i \cdot \Delta\phi_d + \mu_{att}\right) \quad (1)$$

where c_∞ is the outside salt concentration, z_i is the valency of the ion, and $\Delta\phi_d$ the Donnan potential, i.e., the potential increase when going from outside to inside the carbon particle. This is a dimensionless number and can be multiplied by the thermal voltage $V_T=RT/F$ (~25.7 mV) to obtain the Donnan voltage with dimension V. The non-Boltzmann energy term μ_{att} is dimensionless and can be multiplied by RT to obtain a molar energy with dimension J/mol. We will assume equal values of μ_{att} for anion and cation [36]. Inside the carbon micropores, the micropore ionic charge density (per unit micropore volume, dimension mol/m^3=mM) is given by

$$\sigma_{mi} = \sum_i z_i \cdot c_{mi,i} \,. \tag{2}$$

This ionic charge σ_{mi} is compensated by the electronic charge in the carbon matrix: $\sigma_{mi}+\sigma_{elec}=0$. When using this simple equation we exclude chemical surface charge effects, but such effects can be included [42,43]. Next, the ionic charge density relates to the Stern layer potential difference, $\Delta\phi_{St}$, according to

$$\sigma_{mi} = -C_{St,vol} \cdot \Delta\phi_{St} \cdot V_T / F \tag{3}$$

where $C_{St,vol}$ is a volumetric Stern layer capacity in F/m^3. For $C_{St,vol}$ we use the expression

$$C_{St,vol} = C_{St,vol,0} + \alpha \cdot \sigma_{mi}^2 \tag{4}$$

where the second term is included to account for the experimental observation that the Stern layer capacity slightly goes up with micropore charge [36]. From this point onward we assume symmetry and only describe an experiment with two equal electrodes (equal mass and composition) [42]. We describe in this section salt adsorption and charge in a CDI-cycle operating at two discrete values of the cell voltage V_{cell}, namely V_{ch} and V_{disch} (for “charge” and “discharge”), where at both levels equilibrium is established.

Combination of Eqs. (1) and (2) leads to

$$\sigma_{mi} = c_{cation,mi} - c_{anion,mi} = -2 \cdot c_\infty \cdot \exp(\mu_{att}) \cdot \sinh(\Delta\phi_d) \tag{5}$$

and

$$c_{ions,mi} = c_{cation,mi} + c_{anion,mi} = 2 \cdot c_\infty \cdot \exp(\mu_{att}) \cdot \cosh(\Delta\phi_d) \,. \tag{6}$$

The above equations must be supplemented with

$$V_{cell} / V_T = 2 \cdot |\Delta\phi_d + \Delta\phi_{St}| \tag{7}$$

where V_{cell} is either V_{ch} or V_{disch}. In the i-mD model [36], in contrast to the previous mD-model [1,11, 27,42,43,44,45,46,47], the energy term μ_{att} is not taken as a constant, but is given by the ratio of an energy density E divided by the total micropore ions concentration, $c_{ions,mi}$,

$$\mu_{att} = E / c_{ions,mi} \,. \tag{8}$$

This modification, used in the i-mD model, has a significant effect in improving the precision of the mD-model, especially to describe the influence of salinity (see Fig. 4 in ref. [36]) without introducing an extra “fit” parameter. As ref. [36] demonstrated, the use of Eq. (8) gives an excellent description of equilibrium data in CDI, both for salt adsorption and charge, as function of both external salt concentration and of cell voltage.

To calculate the charge Σ_F that is transferred from one electrode to the other during charging (denoted by superscript "ch"), and back during discharging ("disch"), we multiply the micropore charge density σ_{mi} in one electrode, by the volume of micropores per gram of electrode, υ_{mi}, and by Faraday's number *F*, do this for charging and discharging, and take the magnitude of the difference

$$\Sigma_F = \tfrac{1}{2} \cdot F \cdot \upsilon_{mi} \cdot \left| \sigma_{mi}^{ch} - \sigma_{mi}^{disch} \right| \tag{9}$$

where Σ_F has dimension C/g. For the salt adsorption of a cell pair we have

$$\Gamma_{m,salt} = \tfrac{1}{2} \cdot M_{w,NaCl} \cdot \upsilon_{mi} \cdot \left(c_{ions,mi}^{ch} - c_{ions,mi}^{disch} \right) \tag{10}$$

which has dimension g/g ($M_{w,NaCl}$=58.44 g/mol). In Eqs. (9) and (10) the factor ½ stems from the convention in CDI to define salt adsorption and charge by the mass of anode and cathode together.

The charge efficiency Λ is the ratio of salt adsorption over charge transfer in a CDI-cycle, and is given by

$$\Lambda = \frac{F}{M_{w,NaCl}} \cdot \frac{\Gamma_{m,salt}}{\Sigma_F} \,. \tag{11}$$

In case c_∞^{ch}=c_∞^{disch} (the external salt concentration is the same before and after charging, as in the Single Pass-method where the inflow salt concentration is always the same), and we discharge at zero cell voltage, which in our model implies $\sigma_{mi}^{disch} = 0$ and thus $\Delta\phi_d^{disch}$=0, Eq. (11), with the substitution of Eqs. (5), (6), (9) and (10), results in [1,36,42,44]

$$\Lambda = \frac{c_{ions,mi}^{ch} - c_{ions,mi}^{disch}}{\left| \sigma_{mi}^{ch} \right|} = \frac{\cosh\left(\Delta\phi_d^{ch} \right) - \exp\left(\mu_{att}^{disch} - \mu_{att}^{ch} \right)}{\sinh\left(\left| \Delta\phi_d^{ch} \right| \right)} \tag{12}$$

which clearly shows the general feature that the theoretically predicted value for the charge efficiency directly depends on the diffuse layer (Donnan) voltage during charging, $\Delta\phi_d^{ch}$, and not on parameters related to the Stern layer. Note that in the i-mD model, where μ_{att} depends on $c_{ions,mi}$ (which in turn depends on $\Delta\phi_d^{ch}$), charge efficiency is no longer given by $\Lambda = \tanh\left(\left| \Delta\phi_d^{ch} \right| / 2 \right)$ as it is in the mD-model which uses a fixed value of μ_{att} [45,46].

CDI porous electrode transport theory. To describe the dynamics of salt electrosorption and charge in porous carbon film electrodes forming a CDI cell, we jointly consider ion transport through the space between the carbon particles, that is, through the large transport pathways across the electrode (interparticle pore volume), which we call the macropores (subscript: mA), and the electrosorption of ions inside carbon particles (intraparticle pore volume) which we call the micropores (subscript: mi) [43,47,48]. This classical model considers a perfect bimodal pore size distribution, of one type of macropore and one type of micropore, and neglects mesopores [41,49]. In the present work these mesopores are introduced in Eq. (14). Note again that the nomenclature for these pore classes is based here on that in transport theory, not the IUPAC definition based on pore size [1,41]. This mesoporosity describes a charge-neutral volume inside carbon particles, having the same salt concentration as the nearby macropores, but without sustaining ion transport. Ion adsorption in the micropores is described by the i-mD model discussed in the above section. The CDI porous electrode

transport theory describes ion electromigration through the spacer and electrode macropores, and the subsequent storage of ions and electrical charge in the EDLs in the micropores [46]. The geometry considered is based on two porous electrodes placed parallel, with a flat planar slit, called the transport channel or spacer, placed in between. In the direction of flow, this transport channel is mathematically divided into *M* sequential sub-cells, see Fig. 2 in ref. [27] and Fig. 2 in ref. [46]. In the following section, we first describe a single sub-cell and the ion transport into the electrode. Next we describe how all sub-cells can be combined in a unified model for the full CDI system. We focus on a monovalent salt solution, assuming that the two ion diffusion coefficients are equal (as for KCl). Extensions to mixtures with ions of different diffusion coefficients (as must formally also be considered for NaCl) are described in refs. [43,44].

In the CDI porous electrode transport model, two coupled one-dimensional partial differential equations must be solved along with additional algebraic equations to evaluate the transport and adsorption of salt across the porous carbon electrodes. The model describes, as a function of the depth in the electrode x, and time t, four coupled variables: (1) the salt concentration in the macropores, c_{mA}; (2) the electrostatic potential there, ϕ_{mA}; (3) the charge density in the micropores, σ_{mi}; and (4) the ions concentration in the micropores, $c_{\mathrm{ions,mi}}$.

The spacer channel between the two electrodes is described as a series of continuously stirred sub-cells with a salt concentration c_{sp} that is only a function of time, described by the salt mass balance

$$p_{\mathrm{sp}} V_{\text{sub-cell}} \frac{\partial c_{\mathrm{sp}}}{\partial t} = -J_{\mathrm{ions}} A + \phi_{\mathrm{v}} \left(c_{\mathrm{sp,in}} - c_{\mathrm{sp}} \right) \tag{13}$$

where $V_{\text{sub-cell}}$ (in m^3) is the geometrical volume of the sub-cell, p_{sp} is the open porosity of the spacer channel, A the exchange area of one sub-cell with one electrode (in m^2), and ϕ_{v} the water volumetric flow rate running through the cell, i.e., along the electrodes (in m^3/s). We assume the two electrodes to behave symmetrically and as a consequence the ion flux into one electrode, J_{ions}, is equal to the salt flux into both electrodes.

Base on the Nernst-Planck equation [50], transport within the porous electrode is described by two coupled partial differential equations. First, a differential salt mass balance can be set up, given by

$$\frac{\partial}{\partial t}\left(\left(p_{\mathrm{mA}} + p_{\mathrm{meso}} \right) c_{\mathrm{mA}} + \tfrac{1}{2} p_{\mathrm{mi}} c_{\mathrm{ions,mi}} \right) = p_{\mathrm{mA}} D \frac{\partial^2 c_{\mathrm{mA}}}{\partial x^2} \tag{14}$$

with the electrode position x between $0<x<L_{\mathrm{elec}}$, where L_{elec} is the electrode thickness, and where D is the average ion diffusion coefficient in the macropores, and where p_{mA}, p_{meso}, and p_{mi} are the macro-, meso-, and microporosity in the electrode. As Eq. (14) shows, we consider all fluxes to be in only one direction, namely the direction into the electrode, i.e., at cross-angles with the general flow direction of the solution through the channel, see Fig. 2 in Porada *et al*. [46].

The second partial differential equation describes the charge in the micropores and is given by

$$p_{\mathrm{mi}} \frac{\partial \sigma_{\mathrm{mi}}}{\partial t} = 2 p_{\mathrm{mA}} D \frac{\partial}{\partial x}\left(c_{\mathrm{mA}} \frac{\partial \phi_{\mathrm{mA}}}{\partial x} \right). \tag{15}$$

At each position in the electrodes, the macropore potential ϕ_{mA} is related to the potential ϕ_1 in the carbon matrix according to

$$\phi_1 - \phi_{\mathrm{mA}} = \Delta\phi_{\mathrm{d}} + \Delta\phi_{\mathrm{St}} \tag{16}$$

with expressions for $\Delta\phi_{\mathrm{d}}$ and $\Delta\phi_{\mathrm{St}}$ given by Eqs. (3)-(6). At each position the micropore ions concentration $c_{\mathrm{ions,mi}}$ is related to charge σ_{mi} according to

$$c_{\mathrm{ions,mi}}^2 = \sigma_{\mathrm{mi}}^2 + \left(2 \cdot c_{\mathrm{mA}} \cdot \exp\left(\mu_{\mathrm{att}} \right) \right)^2 . \tag{17}$$

With the potential in the carbon matrix set to zero (ϕ_1=0), the cell voltage is given by

$$V_{\mathrm{cell}} = 2 \cdot V_{\mathrm{T}} \cdot \left(\phi_{\mathrm{mA}}\big|_{x=0} + \Delta\phi_{\mathrm{sp}} \right) \tag{18}$$

where "x=0" refers to the front side of the electrode (in contact with the spacer channel), and where $\Delta\phi_{\mathrm{sp}}$ is the voltage drop across half the spacer channel, obtained from

$$J = -4 c_{\mathrm{sp}} p_{\mathrm{sp}} D \cdot L_{\mathrm{sp}}^{-1} \cdot \Delta\phi_{\mathrm{sp}} \tag{19}$$

where J is the current density (in mol/m^2/s). The ions flux, J_{ions}, out of the spacer channel required in Eq. (13) is equal to the ions flux directed into the electrode

$$J_{\mathrm{ions}} = -2 p_{\mathrm{mA}} D \left. \frac{\partial c_{\mathrm{mA}}}{\partial x} \right|_{x=0} \tag{20}$$

and a similar relation holds for the current density,

$$J = -2 p_{\mathrm{mA}} D \left. \left(c_{\mathrm{mA}} \frac{\partial \phi}{\partial x} \right) \right|_{x=0} . \tag{21}$$

For an overview of the required initial and boundary conditions in c_{mA}, ϕ_{mA}, σ_{mi} and $c_{\mathrm{ions,mi}}$ in each sub-cell, see Suppl. Inf. in Porada *et al*. [46]. In the full model for the CDI-cell, M of the sub-cells as described above, are placed sequentially in the direction of flow. In this direction salt is transported through the spacer channel downstream, as described by Eq. (13) with c_{sp} the concentration in sub-cell i and $c_{\mathrm{sp,in}}$ the concentration in the up-stream sub-cell i-1. The concentration in the last sub-cell (i=M) is equal to the effluent concentration. The sub-cell volume is equal to the total spacer channel volume (height times electrode area) divided by the number of sub-cells, M. In the present work we do not include a "dead volume" after the stack as in refs. [42,46]. The current density per cell, I (in A/m^2) is calculated from I=F/M·$\Sigma_{\mathrm{i}}J_{\mathrm{i}}$, where Σ_{i} is a summation over all sub-cells. This current density, I, can be integrated over time and multiplied by the cell cross-sectional area to obtain the total stored charge. The charge stored in an electrode can also be calculated by averaging the local charge density σ_{mi} (Eq. 15) and multiplying by Faraday's number, the microporosity p_{mi}, and the volume of the electrode. Dividing by electrode mass (anode and cathode together) gives us the charge Σ_{F} (C/g) as plotted in Figs. 2, 3 and 4.

Experimental

Electrode preparation. Carbon composite electrode was fabricated using YP-50F (Kuraray, Japan), carbon black (Vulcan XC72R, Cabot Corp., Boston, MA), and a binder (85:5:10 in weight ratio). In order to prepare the binder solution (3 wt%), polyvinylidene fluoride (PVDF, Kynar HSV 900, Arkema Inc., Philadelphia, PA) was dissolved in N-methyl-2-pyrrolidone (NMP) and vigorously stirred for 24 h to secure homogeneity. After YP-50F and carbon black were mixed with the prepared binder solution, it was intensively blended in a ball-milling machine for 40 min (500 rpm) and the resulting carbon slurry was used for casting. The electrode casting was carried out on a glass plate with a doctor blade (thickness 500 μm). Afterwards, the electrode was directly transferred into deionized water together with the glass plate to solidify the binder. The resulting carbon electrode (~260 μm) was cut into square pieces (6×6 cm^2) with a small square (1.5×1.5 cm^2) located at the center.

Table 1. System and electrode dimensions, operational parameters, and settings for theoretical calculations.

	Experimental parameters		
N_s	Number of cells in the CDI stack	4	
ρ_{el}	Electrode mass density	0.41	g mL^{-1}
A_{cell}	Electrode geometric surface area	33.75	cm^2
L_{sp}	Spacer channel thickness (when compressed)	250	μm
p_{sp}	Spacer channel porosity (when compressed)	0.50	
ϕ_v	Flowrate through the CDI stack	30	mL min^{-1}
T	Temperature	298	K
c_∞	Inlet NaCl salt concentration	5, 20, 80	mM
	Values for use in EDL and transport theory		
υ_{mi}	Micropore volume	0.40	mL g^{-1}
p_{mi}, p_{meso}, p_{mA}	Micro-, meso- and macroporosity	0.160, 0.068, 0.566	
D	Average diffusion coefficient of Na^+ and Cl^- (in free solution)	$1.68*10^{-9}$	$m^2 s^{-1}$
$C_{St,vol,0}$	Volumetric Stern layer capacitance in the zero-charge limit	0.17	GF m^{-3}
α	Parameter for non-constant contribution to Stern capacitance	20	F m^3 mol^{-2}
E	Micropore ion-correlation energy	220	kT mol m^{-3}
M	Number of mathematical subcells in the model	1	

CDI experiments. Fig. 1a shows a schematic diagram of the CDI system used in this study. Each cell consists of a pair of graphite current collectors, a pair of carbon electrodes, and a spacer (AP20, Glass Fiber Filter, Millipore, MA, uncompressed thickness ~380 μm). A stack was constructed of N_s=4 of such cells and installed in a rectangular Teflon housing which was sealed off. As depicted in Fig. 1a, water is pumped from outside to inside through the spacer using a peristaltic pump (flow rate 30 mL/min for the stack of 4 cells), and the outlet conductivity and pH were continuously monitored. The experiments were conducted in NaCl solutions of different concentration (c_∞=5, 20, 80 mM) prepared in a vessel (10 L) with N_2 purging. While the solution flows through the CDI stack, the system was controlled by a power supply (IviumStat, Ivium Technologies, the Netherlands). The following voltage differences across each cell were imposed: a voltage V_{ch} during charging (deionization, salt adsorption) and V_{disch} during discharge (regeneration, desorption). For the equilibrium experiments (Figs. 3 and 4) the duration of each step (half-cycle time, or HCT) was 20 min while HCT was lower (but again the same for charging and discharging) in the experiments of Fig. 5. Each experiment was

carried out at a distinct value of V_{disch}, ranging from 0 to 0.9 V, while the charging voltage V_{ch} was always set to 1.2 V as described in Fig. 1b (except for experiments reported in Fig. 2 and Fig. 6). From the measured electrical current, the charge transferred (back and forth) in one cycle is calculated, while from the measured conductivity (corrected via the measured pH for the partial conductivity of protons and hydroxyl ions) and from the water flow rate, the salt adsorption is calculated. Note that salt adsorption in mg/g of NaCl is based on the mass of all electrodes in the system (both anode and cathode). The charge was obtained from the charging step (from integrating the current vs. time-plot), after subtracting a small leakage current, which is the current which still flows when equilibrium is reached after 20 min. Note that when the leakage current would not be accounted for, the calculated charge is a few percent higher, and thus values of the charge efficiency are a few percent less than reported. The charge transfer during discharge is generally a few percent lower than charge transfer in the charging step, i.e., the Coulombic efficiency is below 100%. Charge efficiency, Λ, is the salt adsorption divided by charge, see Eq. (11). None of the reported results are from the first or second cycle after a new experiment, as then dynamic equilibrium is not yet established and the charging salt adsorption and charge are not yet the same as the values during discharge. This condition of salt balance and charge balance is well achieved in subsequent cycles.

To calculate the salt adsorption per cycle, as required in Figs. 5a and 5b, we use the "new data analysis approach" discussed in ref. [28], where the salt adsorption is based on the entire time period that the effluent salt concentration is below the inflow concentration (period from A to B in Fig. 3 in ref. [28]), a period which is slightly delayed relative to the period of cell charging. Instead, in prior work discussing short cycle times [25,27,45] salt adsorption (desorption) was calculated based on the period of cell charging (discharging).

Data analysis to derive EDL-properties. To fit the i-mD model (EDL theory) to the data, four parameters must be adjusted as summarized in Table 1: υ_{mi}, E, $C_{St,vol,0}$ and α. The analysis is based on the following procedures. First of all, we note that predictions of the theory for Λ, or $\Gamma_{m,salt}$, as function of Σ_F (and vice-versa) depend on the micropore volume υ_{mi} and on the energy E, but are independent of the Stern layer parameters $C_{St,vol,0}$ and α. Thus, we first plot data for $\Gamma_{m,salt}$ versus Σ_F (not shown, but similar to Fig. 3g in ref. [36]) and compare with the i-mD model to find appropriate values for E and υ_{mi}. A second comparison considers the interesting fact that the Donnan potential, $\Delta\phi_d$ which uniquely determines Λ, also uniquely relates both $c_{ions,mi}$ and σ_{mi} to one another, see Eqs. (5) and (6) (with the energy E as parameter) and therefore describes the cell voltage V_{cell} (including in the fit $C_{St,vol,0}$ and α), all independent of the value of υ_{mi}. This is also the case for non-zero values of V_{disch}. So fitting theory for $\Lambda(V_{ch},V_{disch})$ to data does not require information of υ_{mi}, see Fig. 3d and 4d. Together with the direct comparisons of $\Gamma_{m,salt}$ and Σ_F vs V_{cell}, we therefore have various parallel methods for reliable data fitting, and as Figs. 3 and 4 demonstrate, across a large dataset (varying c_∞, V_{ch} and V_{disch}), we can very satisfactorily fit all data of $\Gamma_{m,salt}$ and Σ_F using the i-mD model. The EDL parameters we obtain are close to those previously derived in refs. [27,36] where a commercial activated carbon-based electrode was considered.

An important point to note is that the micropore volume of υ_{mi}=0.400 mL/g (per gram electrode) that we use in the theory is less than the total pore volume measured by gas sorption analysis which for Kuraray YP-50 is about 0.67 mL per gram of activated carbon (0.57 mL/g electrode), see refs. [13,46]. Thus, to get an optimum fit of the i-mD model to the data, υ_{mi} is best used as a fitting parameter, not necessarily the same as the total pore volume inside the carbon particles. This is different from our approach in ref. [46] where the pore volume measured by gas adsorption up to pore sizes of 30 nm was included as micropore volume in EDL-modeling and porous electrode (transport) theory. Instead, in the approach as we present here, with υ_{mi} a further fitting parameter, we must consider that the fitted value of υ_{mi} is different from the pore volume from gas adsorption analysis, and we suggest to call this difference (0.57-0.40 mL/g in the present case) mesoporosity. In the mesopores, like in the nearby macropores, we assume equal concentrations of cations and anions (for a 1:1 salt), at the same concentration as in the nearby macropores. The only difference with the macropores is that the ions in the mesopores do not contribute to ion transport across the electrode. The macropore volume, p_{mA}, represents the space located in between the carbon particles and follows from geometrical sizes of the electrodes, the total pore volume from gas sorption analysis, and the skeleton density of the mixture of carbon, carbon black, and binder (for which we use ρ_{sk}=1.93 g/mL). This value is in our case p_{mA}=0.566. Note that the three porosities p_{mA}, p_{meso}, and p_{mi} taken together sum up to a number less than unity (0.794 in the present case), because of the volume taken up by the carbon skeleton itself, by binder and by other solid additives.

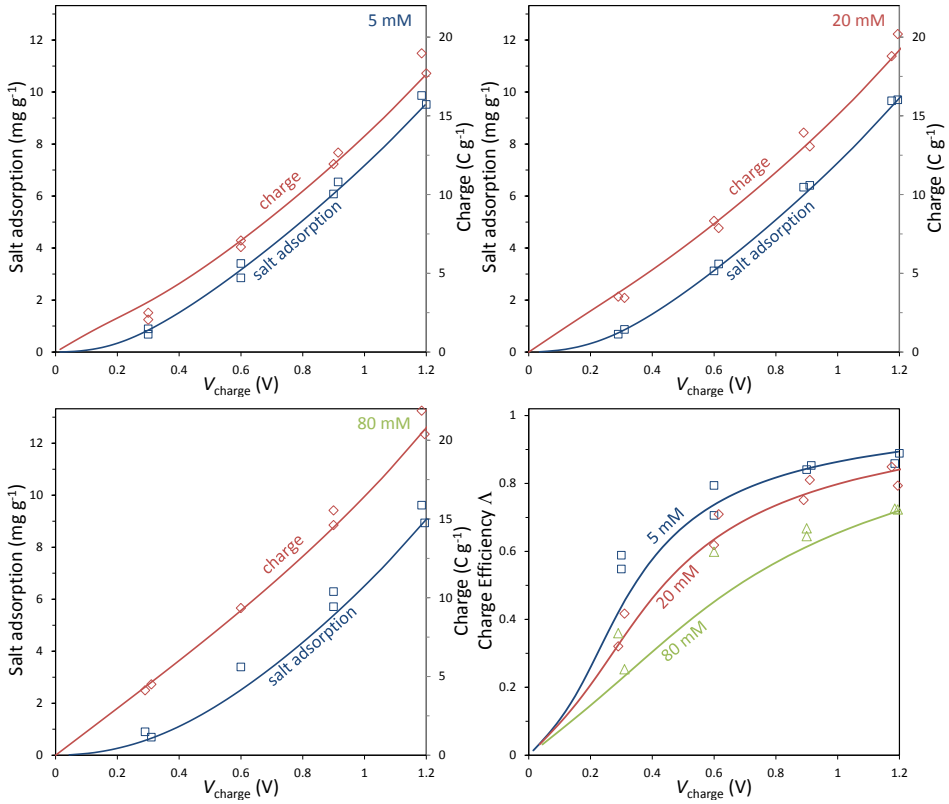

Fig. 3. Equilibrium salt adsorption, charge, and charge efficiency as function of salt concentration and V_{ch}, which is the cell voltage during charging (V_{disch}=0 V). Solid lines obtained according to the i-mD model (parameters in Table 1).

Results and Discussion

To illustrate the response of a CDI cell to the applied cell voltage signal as depicted in Fig. 1b, we show in Fig. 2 the typical CDI behavior of the effluent salt concentration profile over time, and the accumulated charge (current integrated over time), Σ_F. As can be observed, the effluent concentration drops as the charging starts and in time recovers to the initial value, where the area under the base line (dashed line representing the inlet salt concentration) indicates the amount of salt adsorption, $\Gamma_{m,salt}$. Incorporating the factor $F/M_{w,NaCl}$, the ratio of $\Gamma_{m,salt}$ over Σ_F is the charge efficiency, Λ, see Eq. (11). Experimental data for Σ_F, $\Gamma_{m,salt}$ and Λ are further analyzed in Figs. 3-6. An important operational parameter is the half-cycle time (HCT) which in all experiments is the same for charging and discharging (except for the constant-current experiments of Fig. 6). The value of HCT in the experiments reported in Figs. 2-4 is 20 min, while it is reduced to values as low as 1 min in Fig. 5. Because of the long HCT, the data reported in Figs. 3 and 4 can be described by the equilibrium EDL model explained in the first half of the Theory-section, without considering porous electrode ion transport theory which is used in Figs. 5 and 6. Note that in a series of experimental CDI-cycles as reported in Fig. 2, the apparent accumulated charge slowly shifts upward because of a leakage current (see Experimental section). In Fig. 2 this shift is removed in data-processing, and each subsequent charging cycle shifted back to zero charge.

From equilibrium cycles such as reported in Fig. 2, data on salt adsorption $\Gamma_{m,salt}$ and charge Σ_F can be extracted which are reported in Figs. 3 and 4. Fig. 3 shows experimental results (points) and theory (lines) of salt adsorption, charge and charge efficiency as function of the salt concentration and the charging voltage, V_{ch}. Fig. 3 follows the classical operational method of CDI where always V_{disch}=0 V, as for instance in refs. [11,17,25,27,28,42,44,46]. Note that here in Fig. 3 we present data as function of charging voltage, for a larger range of salinities than before [36], from c_∞=5 to 80 mM. Figs. 3a-c show data and theory for salt adsorption in mg/g (left y-axis) and charge in C/g (right y-axis), in such a way that for Λ=1, the two lines (data sets) should overlap. As clearly they do not overlap, the charge efficiency is less than unity, Λ<1. Fig. 3a shows that at the lowest salt concentration of c_∞=5 mM the two lines (data sets) are closest, and Λ is the closest to unity. Figs. 3a-c show that as function of V_{ch}, both Σ_F and $\Gamma_{m,salt}$ increase, but the latter increases faster (relatively) and thus their ratio, which is Λ, increases with V_{ch}. As function of c_∞ (for a given V_{ch}), Σ_F increases while $\Gamma_{m,salt}$ is constant (in the range of c_∞ studied). Thus Λ increases with V_{ch} and decreases with c_∞, as shown in more detail in Fig. 3d. In the present data range, $\Gamma_{m,salt}$ does not vary with c_∞, in line with data in ref. [36] which showed that for even lower and higher c_∞, $\Gamma_{m,salt}$ decreases again. This non-monotonic trend cannot be explained by a simple adsorption isotherm that describes the adsorption of an uncharged solute, which would always predict $\Gamma_{m,salt}$ to increase with c_∞. Instead, the observed dependence of $\Gamma_{m,salt}$ on c_∞ (to first increase, and then to decrease again) is the consequence of the salt storage mechanism in CDI, where salt is stored as individual ions in the electrical double layers of two mutually charged porous electrodes.

Fig. 4 presents results where we fix V_{ch} at 1.2 V and vary V_{disch} for different values of the salt concentration and again plot salt adsorption, charge and charge efficiency. As can be seen, theory

again properly describes the data (parameter settings given in Table 1). Experimentally we observe that the charge efficiency increases with increasing V_{disch}, see Fig. 4d, which is also in alignment with the theoretical predictions. The charge efficiency increases to values close to unity, especially for V_{disch} beyond 0.3 V. In Figs. 4a-4c, the salt adsorption and the charge transfer are separately displayed, where the ratio of these two parameters refers to the charge efficiency. As confirmed in Fig. 4d, we observe that these two parameters (charge and salt adsorption) get closer as V_{disch} increases. As expected, the charge decreases quite linearly when V_{disch} increases (note that the increase in V_{disch} leads to a decrease in the difference V_{ch}-V_{disch}), indicating the typical capacitive behaviour of carbon electrodes. On the other hand, the behaviour of the salt adsorption as a function of V_{disch} is different from that of the charge. In contrast to the dependence of charge on V_{disch}, the salt adsorption in a cycle remains quite invariant with V_{disch}, as long as V_{disch} does not go beyond 0.3 V. This result confirms that charge efficiency can be increased by increasing V_{disch} to values up and including V_{disch}=0.3 V with only a marginal loss of the salt adsorption per cycle. At c_{∞}=20 mM, upon increasing V_{disch} from 0 to 0.3 V, the charge decreases by 20% while the salt adsorption goes down by only 7%. This implies that the charge efficiency goes up by 14%, and thus the energy consumption per ion removed goes down by that number of 14%, as will be explained below.

An explanation for the positive effect of increasing V_{disch} is as follows. When the cell is charged at V_{ch}=1.2 V followed by a discharge at V_{disch}=0 V (following the conventional method), the adsorption of counterions is accompanied by the expulsion of coions, so that the charge efficiency drops to values below unity [37]. This undesirable behaviour of coions can be minimized by increasing the *dis*charge voltage [37,38]. Now, with values of V_{disch} higher than 0 V, a certain amount of coions remains expelled during discharging (is not re-adsorbed). In a next cycle, therefore, the expulsion of coions is small when the charging starts from a value of V_{disch} higher than 0 V, and thus most of the electrical charge transferred between the two electrodes is utilized solely for the adsorption of counterions.

The increased value of charge efficiency directly implies a reduction in the required energy per ion removed. This can be understood as follows. Because the adsorption operates at constant charging voltage, the energy input is directly proportional to the quantity of charge transfer, and thus is inversely proportional to the charge efficiency Λ. For example, for the data at c_{∞}=20 mM, the energy costs per ion removed is ~30 kT at V_{disch}=0 V, and decreases to ~26 kT for V_{disch}=0.3 V, a reduction by 14%. In this calculation we have not included possible energy recovery during discharge, which is possible when V_{disch}>0 V [51]. Indeed, for this situation of V_{disch}=0.3 V, assuming perfect energy recovery during discharge, the energy per ion removed is reduced to ~20 kT, a reduction of about 30% compared to the original value at V_{disch}=0 V. Note that for the separation that was achieved, the thermodynamic minimum energy input (decrease in mixing entropy) is only about 0.2 kT per removed ion, a factor 100 below the actual energy input.

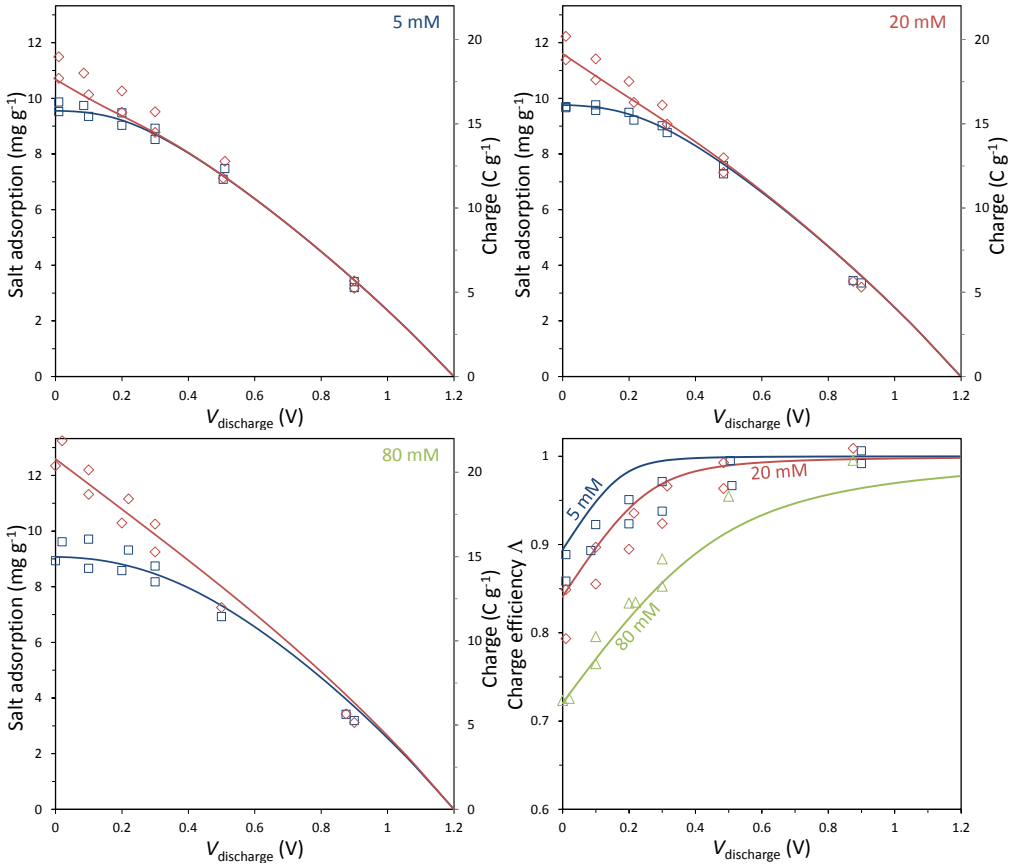

Fig. 4. Salt adsorption, charge, and charge efficiency (Λ) as function of salt concentration and discharge voltage, V_{disch} (V_{ch}=1.2 V). Solid lines obtained according to the i-mD model (parameters in Table 1).

Figs. 3 and 4 discussed equilibrium EDL-properties. The next task is to analyse the kinetics of the CDI process. To this end we first analyze CDI cycles at constant voltage (CV), at increasingly short half-cycle times (HCT), see Fig. 5. In Fig. 5a we plot the average salt adsorption rate, "ASAR" which is the salt adsorption per cycle, divided by the total cycle time, which is twice the HCT.

Fig. 5a clearly demonstrates, both theoretically and experimentally, that ASAR increases with lowering HCT (as also reported in ref. [27]), and in addition that there is hardly an effect of V_{disch}. Admittedly, we had hoped that at an increased V_{disch}, ASAR will be higher, but this is not the case, and ASAR is actually somewhat less. This prior assumption was based on the idea that with V_{disch}=0 V at the start of each charging or discharging step, coions and counterions go in opposite direction through the electrode and into the micropores. This opposite movement would lead to ion-ion friction and thus a retardation in the motion of both types of ions. Increasing V_{disch} would then lead to a situation where only counterions move in and out of the electrode, undisturbed by other ions moving in the opposite direction. However, results in Fig. 5a do not support the hypothesis of a frictional force between ions moving in opposite direction, and apparently this suggested retardation effect is not there, or at least is not strong. The transport model doesn't include such an effect either, and describes data very well.

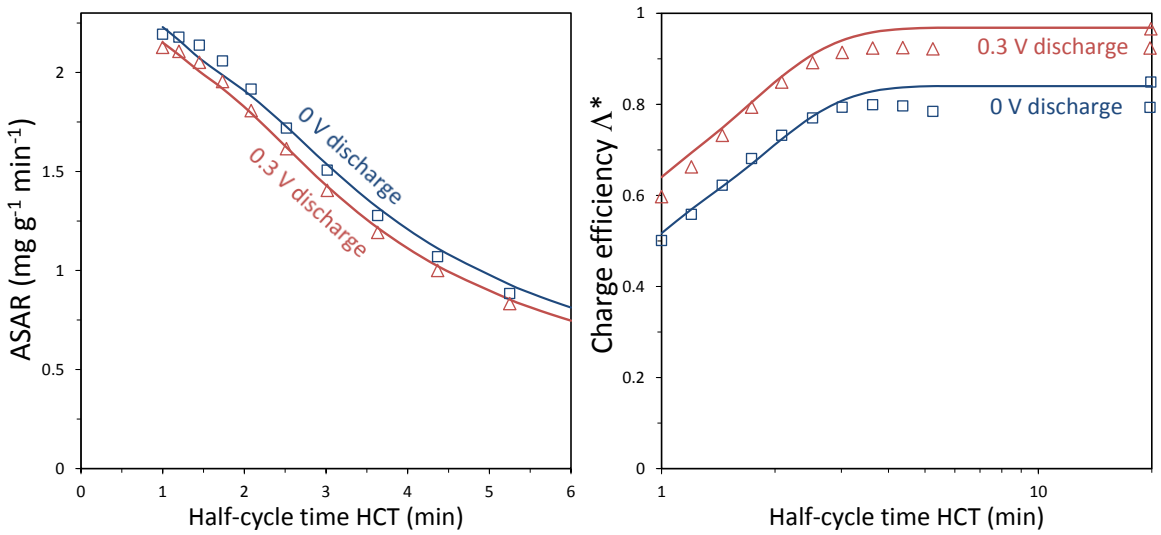

Fig. 5. CDI at short cycle times. (a). Average salt adsorption rate as function of half-cycle time (HCT; charging and discharging step of equal duration, namely equal to HCT) and as function of V_{disch}. (b). Dynamic charge efficiency as function of HCT (V_{ch}=1.2 V, c_{∞}=20 mM, electrode thickness 235 μm).

Analyzing both the charge transfer Σ_F and salt adsorption $\Gamma_{m,salt}$ per cycle, Fig. 5b shows results of the ratio of the two, the "dynamic" charge efficiency, Λ^*. Here we add the prefix "dynamic" because in contrast to the results of Fig. 3 and 4, here the charge efficiency is based on a CDI cycle that is not yet at equilibrium. Consequently, the theory lines for Λ^* in Fig. 5b are not based on an equilibrium EDL model but are based on the transport model. Both in theory and data, Fig. 5b shows that shorter cycles result in a lower Λ^* (vs. the values at longer HCT) indicating an increase in energy costs per ion removed. This is the case because the required energy per amount of salt removed is inversely proportional to Λ^* for a fixed charging voltage. As in Fig. 4, we observe that operation at V_{disch}=0.3 V gives a higher charge efficiency, and thus the same energetic advantage of operation at increased values of V_{disch} remains, of about 14% without energy recovery and 30% with energy recovery.

Finally, we show results for constant-current (CC) operation during charging in Fig. 6. Constant-current operation is advantageous over constant-voltage (CV) because it leads to a constant effluent salt concentration, $c_{eff,level}$, that can be easily tuned by adjusting the current [25]. However, up to now it was argued that this operational mode is only feasible with ion-exchange membranes incorporated in CDI (membrane-CDI), because without membranes (i.e., in normal CDI) it takes a longer time before $c_{eff,level}$ is reached after switching the current direction, see Fig. 8 in ref. [1]. In Fig. 6 we show our results aiming at reducing the time for $c_{eff,level}$ to be reached. In these experiments with CC operation during charging (with a constant current of 0.41 A applied to the stack of N_s=4 cells, thus at a current density of 30.6 A/m^2, until a cell voltage of V_{cell}=1.4 V is reached), the discharge step is always defined by CV operation at certain values of V_{disch}, always for a duration of 250 s. Fig. 6a demonstrates that a more rapid drop of salt concentration to $c_{eff,level}$ is found with increasing V_{disch}, both in the experimental data (points) and in the theoretical calculations (lines). This is due to the fact that at V_{disch}=0 V, at the start of a new charging step, coions and counterions replace one another, a phenomenon called "ion swapping" in ref. [52] without resulting desalination. Instead, with increasing

V_{disch} we reach the situation that right after start of a new cycle only counterions are adsorbed (with coions remaining outside the micropores at all times).

Fig. 6a also shows a theory line for the case that for a short duration of about 20 s after start of the charging step, we use a twice-higher value of the current. The current vs. time-curve is $I(t)=I_{final}*(2\alpha*(1-\tanh(\alpha*(t-\beta)))+1)$, $\alpha=1/4$, $\beta=22$. This modification (in combination with V_{disch}=0.3 V) results in reaching the value $c_{eff,level}$ even more rapidly. Note that the theoretical calculations for Fig. 6 are based on Φ=27.5 mL/min (for the stack of 4 cells), instead of Φ=30 mL/min, to make the theory-lines fit the data somewhat better. Thus these calculations must not be considered as exact, but as illustrative. Fig. 6b shows that considering only the first 100 s of charging, the dynamic charge efficiency Λ^* increases significantly with discharge voltage. As the total charge input is constant (41 C), this implies that the desalination also increased in the same way. In this case, however, the energy consumption is not inversely proportional to Λ^* as it is in Fig. 5, because the cell voltage is no longer constant. Instead, Fig. 6c shows how for CC operation the energy consumption (without energy recovery) is rather invariant with V_{disch}. Interestingly, both theory and data predict a shallow minimum in the energy consumption, though at a different value of V_{disch}.

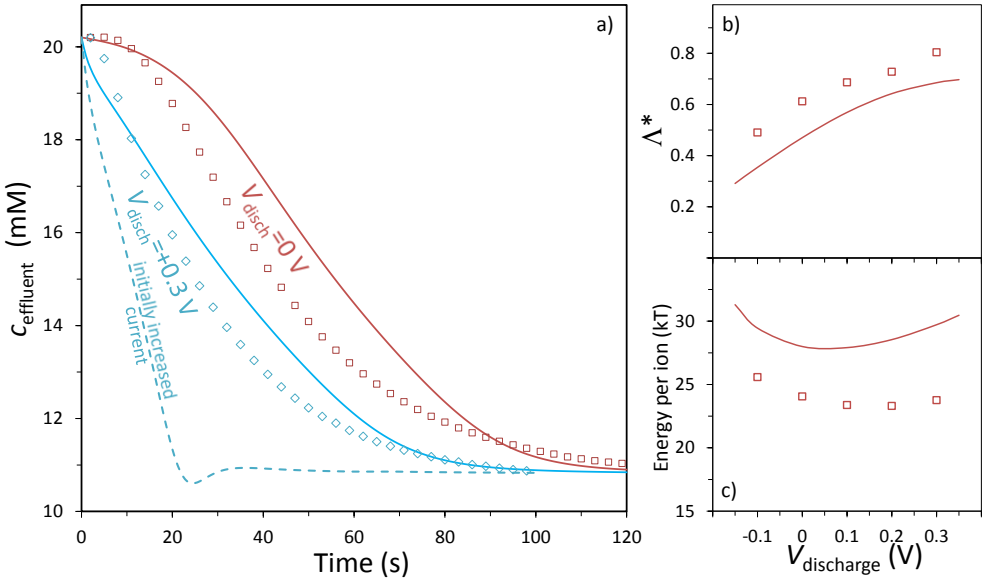

Fig. 6. Constant-current CDI operation. a) Effluent salt concentration as function of V_{disch} (data represented by dots; theory calculations by lines). b) Dynamic charge efficiency vs. V_{disch}. c) Electrical energy input per ion removed (kT) vs. V_{disch}. (I_{ch}=30.6 A/m^2, c_∞=20 mM, electrode thickness 320 μm).

Conclusions

In this work, we have demonstrated that the charge efficiency of a CDI cycle can be improved by increasing the discharge voltage V_{disch}. In constant voltage (CV) operation, V_{disch} up to 0.3 V was promising since the charge efficiency was significantly enhanced while the salt adsorption only minutely decreased. Another important finding was kinetics in constant-current (CC) operation: the constant level in effluent salt concentration, which is the key advantage of CC operation, was more rapidly reached when V_{disch} was increased to a value higher than zero. For CV operation, the required energy input per ion removed went down significantly when we increased the discharge voltage, for

our standard experimental settings by about 14% without energy recovery during discharge, and by 30% with perfect energy recovery.

The improved modified (i-mD) Donnan model described the full experimental data set of equilibrium salt adsorption and charge to an excellent degree. Including the i-mD model in a porous electrode transport theory resulted in a dynamic theory that well illustrates several of the observed dynamic features of ion transfer and charge storage, both for constant-voltage and constant-current operation. In conclusion, our work showed that to increase system performance of CDI, there are many more options open besides developing new electrode materials, or the development of improved membranes. We demonstrate that by carefully adjusting voltage and current levels in a CDI-cycle, salt adsorption per unit charge transferred can be significantly increased, as well as the rate by which (in CC operation) a constant salt effluent level is reached.

Acknowledgments

This work was performed in the cooperation framework of Wetsus, centre of excellence for sustainable water technology (www.wetsus.nl). Wetsus is co-funded by the Dutch Ministry of Economic Affairs and Ministry of Infrastructure and Environment, the European Union Regional Development Fund, the Province of Fryslân, and the Northern Netherlands Provinces. This project is supported by Korea Ministry of Environment as “Converging Technology Project (2014001640002)”. The authors like to thank the participants of the research theme Capacitive deionization for the fruitful discussions and their financial support. We especially thank Karel Keesman (Wageningen University) for his ongoing support in the numerical modeling of porous electrode theory.

References

1. S. Porada, R. Zhao, A. van der Wal, V. Presser, P.M. Biesheuvel, *Progress in Materials Science* **58** (2013) 1388.
2. H.-H. Jung, S.-W. Hwang, S.-H. Hyun, K.-H. Lee, G.-T. Kim, *Desalination* **216** (2007) 377.
3. R. Rica, R. Ziano, D. Salerno, F. Mantegazza, D. Brogioli, *Phys. Rev. Lett.* **109** (2012) 156103.
4. Z.H. Huang, M. Wang, L. Wang, F.Y. Kang, *Langmuir* **28** (2012) 5079.
5. H.B. Li, C.Y. Nie, L.K. Pan, Z. Sun, *Desalination and Water Treatment* **42** (2012) 210.
6. Ch.-H. Hou, Ch.-Y. Huang, *Desalination* **314** (2013) 124.
7. G. Wang, B. Qian, Q. Dong, J. Yang, Z. Zhao, J. Qiu, *Sep. Purif. Techn.* **103** (2013) 216.
8. X. Gao, A. Omosebi, J. Landon, K. Liu, *Electrochem. Comm*. **39** (2014) 22.
9. T. Kim and J. Yoon, *J. Electroanal. Chem*. **704** (2013) 169.
10. Y.A.C. Jande, W.S. Kim, *Sep Purif Techn.* **115** (2013) 224.
11. S. Porada, B.B. Sales, H.V.M. Hamelers, P.M. Biesheuvel, *J. Phys. Chem. Lett*. **3** (2012) 1613.
12. S.I. Jeon, H.R. Park, J.G. Yeo, S. Yang, C.H. Cho, M.H. Han, D.K. Kim, *Energy & Environmental Sci*. **6** (2013) 1471.
13. S. Porada, D. Weingarth, H.V.M. Hamelers, M. Bryjak, V. Presser, P.M. Biesheuvel, *J. Mater. Chem. A* **2** (2014) 9313.
14. S.-I. Jeon, J.-G. Yeo, S.C. Yang, J. Choi, D.K. Kim, *J. Mater. Chem. A.* **2** (2014) 6378.
15. K.B. Hatzell, E. Iwama, A. Ferris, B. Daffos, K. Urita, Th. Tzedakis, F. Chauvet, P.-L. Taberna, Y, Gogotsi, P. Simon, *Electrochem. Comm.* **43** (2014) 18.
16. Y. Gendel, A.K.E. Rommerskirchen, O. David, M. Wessling, *Electrochem. Comm.* **46** (2014) 152.

17. M.E. Suss, T.F. Baumann, W.L. Bourcier, C.M. Spadaccini, K.A. Rose, J.G. Santiago, M. Stadermann, *Energy & Environmental Sci.* **5** (2012) 9511.
18. I. Cohen, E. Avraham, M. Noked, A. Soffer, D. Aurbach, *J. Phys. Chem. C* **115** (2011) 19856.
19. J. Liu, S. Wang, J. Yang, J. Liao, M. Lu, H. Pan, L. An, *Desalination* **344** (2014) 446.
20. K. Laxman, M.T.Z. Myint, H. Bourdoucen, J. Dutta, *ACS Appl. Mater. Interf*. **6** (2014) 10113.
21. M.C. Zafra, P. Lavela, G. Rasines, C. Macías, J.L. Tirado, C.O. Ania, *Electrochimica Acta* **135** (2014) 208.
22. L. Han, K.G. Karthikeyan, M.A. Anderson, J.J. Wouters, K.B. Gregory, *Electrochim. Acta* **90** (2013) 573.
23. J.-H. Yeo and J.-H. Choi, *Desalination* **320** (2013) 10.
24. B.M. Asquith, J. Meier-Haack, B.P. Ladewig, *Desalination* **345** (2014) 94-100.
25. R. Zhao, P.M. Biesheuvel, A. van der Wal, *Energy & Environmental Sci*. **5** (2012) 9520.
26. Y-J. Kim, J.-H. Kim, J.-H. Choi, *J. Membrane Sci.* **429** (2013) 52.
27. R. Zhao, O. Satpradit, H. Rijnaarts, P.M. Biesheuvel, A. van der Wal, *Water Research* **47** (2013) 1941.
28. R. Zhao, S. Porada, P.M. Biesheuvel, A. van der Wal, *Desalination* **330** (2013) 35.
29. B. van Limpt and A. van der Wal, *Desalination* **342** (2014) 148.
30. Y. Liu, L. Pan, X. Xu, T. Lu, Z. Sun, D.H.C. Chua, *Electrochimica Acta* **130** (2014) 619.
31. A. Omosebi, X. Gao, J. Landon, K. Liu, *ACS Applied Mat. Interfaces* **6** (2014) 12640.
32. T. Kim, H. Yoo, S. Oh, J. Yoon, *Electrochim. Acta* **139** (2014) 374.
33. M. Mossad and L. Zou, *Chem. Eng. J*. **223** (2013) 704.
34. L. Han, K.G. Karthikeyan, M.A. Anderson, K.B. Gregory (2014) *J. Colloid Interface Sci.* **430** (2014) 93.
35. H. Li, F. Zaviska, S. Liang, J. Li, L. He, H.Y. Yang, *J. Mater. Chem. A*. 2 (2014) 3484.
36. P.M. Biesheuvel, S. Porada, M.D. Levi, M.Z. Bazant, *J. Solid State Electrochem.* **18** (2014) 1365.
37. E. Avraham, M. Noked, Y. Bouhadana, A. Soffer, D. Aurbach, *J. Electrochem. Soc*. **156** (2009) P157.
38. I. Cohen, E. Avraham, A. Soffer, D. Aurbach, *ECS Transactions* **45** (2013) 43.
39. Y.A.C. Jande and W.S. Kim, *Desalination* **329** (2013) 29.
40. B. Kastening and M. Heins, *Electrochimica Acta* **50** (2005) 2487.
41. A.M. Johnson and J. Newman, *J. Electrochem. Soc*. **118** (1971) 510.
42. S. Porada, M. Bryjak, A. van der Wal, P.M. Biesheuvel, *Electrochimica Acta* **75** (2012) 148.
43. P.M. Biesheuvel, Y. Fu, and M.Z. Bazant (2012) *Russian Journal of Electrochemistry* **48** 580.
44. R. Zhao, M. van Soestbergen, H.H.M. Rijnaarts, A. van der Wal, M.Z. Bazant, P.M. Biesheuvel, *J. Colloid Interface Sci.* **384** (2012) 38.
45. P.M. Biesheuvel, R. Zhao, S. Porada, A. van der Wal, *J. Colloid Interface Sci.* **360** (2011) 239.
46. S. Porada, L. Borchardt, M. Oschatz, M. Bryjak, J. Atchison, K. Keesman, S. Kaskel, P.M. Biesheuvel, V. Presser, *Energy & Environmental Sci.* **6** (2013) 3700.
47. P.M. Biesheuvel, Y.Q. Fu, and M.Z. Bazant, *Physical Review E* **83** (2011) 061507.

48. K. Sharma, R.T. Mayes, J.O. Kiggans Jr., S. Yiacoumi, J. Gabitto, D.W. DePaoli, S. Dai, C. Tsouris, *Sep Purif Techn*. **116** (2013) 206.

49. M. Yaniv and A. Soffer, *J. Electrochem. Soc*. **123** (1976) 506.

50. V.V. Nikonenko, A.V. Kovalenko, M.K. Urtenov, N.D. Pismenskaya, J. Han, P. Sistat, G. Pourcelly, *Desalination* **342** (2014) 85.

51. M. Alkuran, M. Orabi, 12th International Middle-East Power System Conference MEPCON (2008) 470.

52. P. Wu, J. Huang, V. Meunier, B.G. Sumpter, R. Qiao, *J. Phys. Chem. Lett.* **3** (2012) 1732.